Dawson, G., & Bamber, J. (2017). Antarctic Grounding Line Mapping From CryoSat-2 Radar Altimetry. *Geophysical Research Letters*. https://doi.org/10.1002/2017GL075589

AGU PUBLICATIONS

Geophysical Research Letters

RESEARCH LETTER
10.1002/2017GL075589

Key Points:
- A new method that allows us to map the limit of ice flexure using CryoSat-2 data
- The mapped grounding line is in good agreement with previous DInSAR and ICESat measurements
- Provides additional coverage of the Antarctic grounding zone

Supporting Information:
- Supporting Information S1

Correspondence to:
G. J. Dawson,
geoffrey.dawson@bristol.ac.uk

Citation:
Dawson, G. J., & Bamber, J. L. (2017). Antarctic grounding line mapping from CryoSat-2 radar altimetry. *Geophysical Research Letters*, *44*. https://doi.org/10.1002/2017GL075589

Received 7 SEP 2017
Accepted 15 NOV 2017
Accepted article online 20 NOV 2017

Antarctic Grounding Line Mapping From CryoSat-2 Radar Altimetry

G. J. Dawson[1] **and J. L. Bamber**[1]

[1] Bristol Glaciology Centre, School of Geographical Sciences, University of Bristol, Bristol, UK

Abstract We present a new technique for mapping the grounding line of Antarctic ice shelves using a combination of CryoSat-2 standard and swath elevation data. Our method is based on detecting the tidal signal in pseudo crossovers and is tested on the Siple Coast region of West Antarctica. The mapped grounding line is in good agreement with previous observations from differential SAR interferometry and from ICESat repeat tracks, with a standard deviation of 1.1 km and 1.0 km, respectively, between these methods and ours. There is, however, an average seaward bias of 0.6 km, which is due to the poorer precision of CryoSat-2. We have improved coverage particularly near the Echelmeyer Ice Stream where we have shown that the grounding zone is approximately 25 km inland from previous estimates. This new method is computationally efficient and can be applied to the rest of Antarctica.

1. Introduction

The grounding line is the boundary where the grounded ice sheet detaches from the bed and begins to float. It is the most appropriate boundary for estimating the balance between outgoing ice fluxes and snow accumulation and is the point past which the ocean can influence, and interact with, the ice sheet. Knowledge of its position and dynamics are critical in assessing the stability of the inland ice sheet, for mass budget calculations and as an input into numerical models. Moreover, grounding line retreat in West Antarctica (Christie et al., 2016; Rignot et al., 2014; Scheuchl et al., 2016) and dynamic thinning around the margins of the ice sheet (McMillan et al., 2014; Shepherd et al., 2002) has highlighted the importance of monitoring temporal changes of the grounding line.

The grounding line (point G in Figure 1) is strictly not a single position, but a zone that is modulated on short time scales, by the combined influence of tidal motion and bedrock slope. Various approaches can be used to identify surface features of the grounding zone as a proxy for the grounding line location, based on either tidal flexure of the floating ice or a break-in-slope of the surface (Figure 1). The most reliable approach to date is to identify the inner limit of tide-induced ice sheet flexure (point F in Figure 1), using differential satellite radar interferometry (DInSAR) (Gray et al., 2002; Rignot, 1998). It is also possible to determine the limit of tidal flexure from repeat track analysis of ICESat (Ice, Cloud, and land Elevation Satellite) laser altimetry (Fricker & Padman, 2006). However, both DInSAR and ICESat picks have variable and heterogeneous spatial and temporal sampling and, to date, have been unable to provide a complete grounding line product for Antarctica with a single time stamp (e.g., 1 year). Using satellite imagery (Bindschadler et al., 2011; Bohlander & Scambos, 2007) or satellite altimetry (Bamber & Bentley, 1994; Hogg et al., 2017) to measure the break-in-slope between the flat ice shelf and the steeper ice sheet (point I in Figure 1) provides good spatial coverage but can be difficult to identify in fast-flowing areas with low surface slope. Additionally, the distance from points I to G depends on ice thickness, basal traction, ice speed, and ice rheology and can deviate from methods that infer the grounding line location based on point F by tens of kilometers (Bamber & Bently, 1994; Brunt, Fricker, Padman, & O'Neel, 2010; Depoorter et al., 2013; Fricker & Padman, 2006; Rignot et al., 2011a). As a consequence, the most complete grounding line data set to date is a composite of different techniques from multiple epochs, using point F where available and point I elsewhere (Depoorter et al., 2013).

Satellite radar altimetry has the potential to provide another method to measure point F using either repeat tracks, similar to ICESat, or crossing points of ascending and descending tracks (crossovers). In the past, however, poor performance near breaks in slope has limited the sampling of the grounding zone using conventional satellite radar altimetry (Bamber et al., 2009). CryoSat-2, launched in 2010, performs better over sloping terrain as it uses a synthetic aperture radar interferometric (SARIn) mode near the margins of the ice sheet,

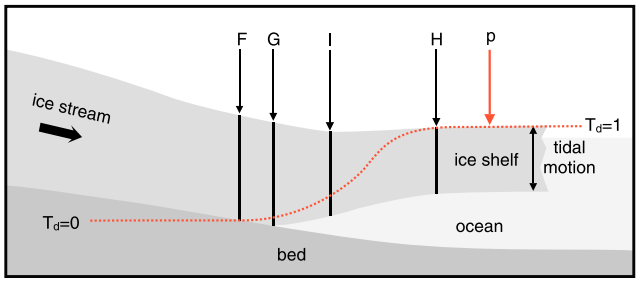

Figure 1. Schematic of an ice shelf grounding zone adapted from Fricker and Padman (2006). Point G is the limit if ice flotation, point F is the limit of tide-induced ice sheet flexure, point I is the break in surface slope, and point H is the inshore limit of hydrostatic equilibrium. The red line shows the expected behavior of the dimensionless tidal amplitude: $T_d = 1$ when the real tidal amplitudes matches the closest model tidal amplitude, p, and $T_d = 0$ on grounded ice.

providing greatly improved sampling (Wang et al., 2015). This study presents a method based on pseudo crossovers (described below), which allows us to map point F using CryoSat-2 data. We chose the Siple Coast region of the Ross Ice Shelf to test this new technique, as there are a range of surface slopes including fast-flowing ice streams with relatively low slope, which have proved challenging for image-based break-in-slope methods (Depoorter et al., 2013).

2. Data and Methodology

We used 3 years of CryoSat-2 SARIn baseline C data spanning from January 2011 to December 2013 in this study. By processing the level 1b data (see the supporting information), we were able to use elevation measurements based on the first return (point of closest approach or POCA) and "swath processed" heights derived from the time-delayed waveform beyond the first return (Gray et al., 2013). Swath data provide elevation estimates downslope of POCA, and where there is a break-in-slope such as the grounding zone, POCA points tend to be clustered upslope on grounded ice. This would limit coverage if we did not combine it with swath data to provide downslope elevation estimates.

To measure the amplitude of the vertical motion due to tides, we adapted the pseudo crossover method of Wouters et al. (2015), as it was appropriate to use with the irregular spatial sampling of CryoSat-2 data. Other methods such as repeat track analysis similar to that used with ICESat data (Fricker & Padman, 2006) or a "conventional" crossover approach, typically used in ocean altimetry, require the reflection point of the return wave to be approximately located at nadir. In sloping terrain, the geocoded elevation measurements from the CryoSat-2 SARIn mode can be several kilometers from the nadir point in the cross-track direction. This, combined with the geodetic orbit (with a 369 day repeat cycle) of CryoSat-2, made these methods unsuitable.

The pseudo crossover method involves determining elevation changes at a given point by collecting observations within a grid cell, and then simultaneously solving for a linear surface elevation rate and topography. We adapted this method by solving for a dimensionless tidal amplitude T_d, instead of a linear surface elevation rate which is unsuitable for measuring an oscillating signal. This method allowed us to measure the contribution of the vertical motion of the tides using data that poorly samples the tidal signal, and effectively removed any effects of aliasing. The dimensionless parameter T_d was scaled by a model tidal amplitude calculated at a constant distance of 10 km from the nominal grounding line in Depoorter et al. (2013) using the CAT2008a tide model, which is an update to the model described by Padman et al. (2002) (Figure 2a). By using a bilinear fit to represent the topography, the elevation h, can be described by

$$h(x, y, p) = a_0 + a_1.x + a_2.y + T_d.p \tag{1}$$

where a_0 is the mean elevation, a_1 and a_2 are the slopes of the topography in the x and y direction, respectively, and p is the model tidal amplitude. This results in T_d being 1 when the real tidal amplitudes match the closest model tidal amplitudes 10 km offshore of the grounding line, and 0 when there is no correlation between elevation and model tidal amplitudes (Figure 1). In the grounding zone, the vertical motion of the ice will still be in phase; however, the amplitude will depend on ice thickness, rheology, and bedrock topography, and T_d will give a measure of the magnitude of the tidal contribution to elevation measurements. Any elevation change not associated with tidal flexure (e.g., from thinning of the ice sheet) will not correlate with tidal motion and will increase the random error in the calculation of T_d. We can include these temporal changes in elevation by adding a linear surface elevation rate to equation (1).

We used a distance of 10 km offshore from the grounding line as, in most cases the ice will be in hydrostatic equilibrium, but still close enough to the grounding zone for its tidal motion to be in phase. Over this distance the tidal amplitude of freely floating ice varies little; hence, the amplitude at point p is approximately equal to the amplitude at the inshore limit of hydrostatic equilibrium (point H in Figure 1). The exact location for our predicted tidal amplitude is therefore not critical as long as it is approximately equal to the amplitude at point H and is not substantially out of phase with the tidal cycle in the grounding zone. The accuracy

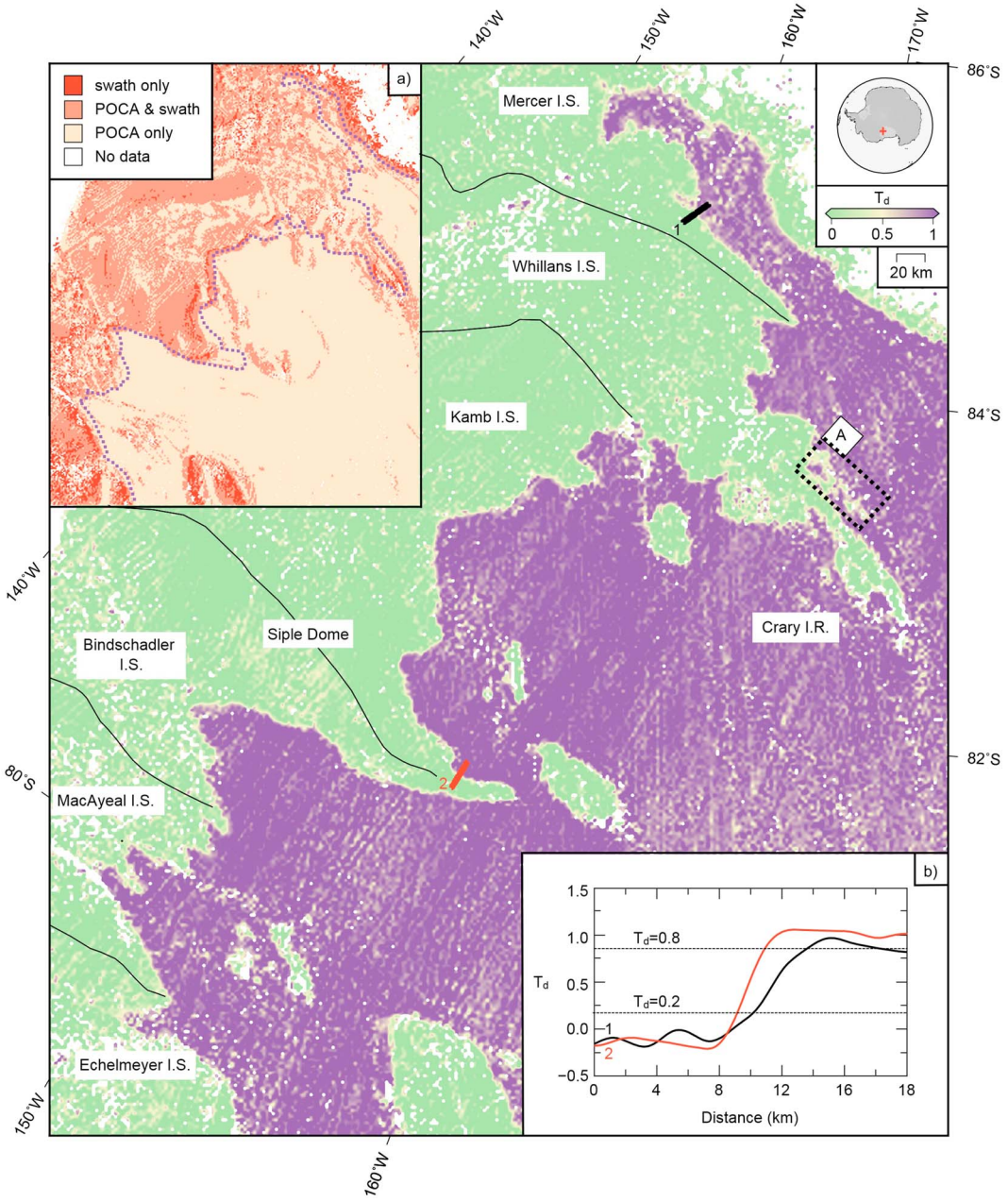

Figure 2. Dimensionless tidal amplitude T_d for the Siple Coast region of the Ross Ice Shelf. Box A highlights an extra area of grounded ice, south of Crary Ice Rise. Inset a) shows where we used POCA, swath or both POCA and swath data to calculate T_d. The blue points are the locations of the predicted tidal amplitudes we used in the calculation of T_d. Inset b) shows cross sections of the Kamb and Mercer Ice Streams. The place labels show ice streams (I.S.) (along with catchment boundaries Mouginot et al., 2017; Rignot et al., 2013) and ice rises (I.R.)

of the CATS2008a tide model (~5 cm, Padman et al., 2008) is below the precision of individual POCA elevation estimates and will not significantly contribute to the error in the calculation T_d.

Within each 2 × 2 km grid cell we used the elevation data, model tidal amplitudes, and equation (1) to simultaneously solve for T_d and topography. To ensure we sampled the tidal signal sufficiently, we only calculated T_d for cells that contained elevation measurements from four different satellite passes. Also, to remove any aliased signals, we only calculated T_d if the range of predicted tidal amplitudes is greater than 0.5 m. This was based on the precision of individual POCA elevation estimates from CryoSat-2 and did not limit the detectable vertical motion in the grounding zone; instead, it set a lower limit to the range of tidal amplitudes of freely

floating ice used when calculating T_d. If any residuals from the fit were greater than 3 median absolute deviations, we removed these points and reran the calculation. This process removed any outliers and was performed iteratively until all residuals were within 3 median absolute deviations. If T_d was anonymously high or low, this was likely a result of erroneous elevation data, leading to a poor fit to equation (1). We considered results valid if $-0.5 < T_d < 1.5$ and if $|T_d - \tilde{T}_d| < 0.5$ where $\tilde{T}_d$ is the median value of neighboring cells.

3. Results

To test our new technique, we chose the Siple Coast region of the Ross Ice Shelf. This area has a tidal range of ~100 to 200 cm, which is close to the average for the Southern Ocean around Antarctica (Figure S1 in the supporting information), and there are a range of surface slopes near the grounding zone. The grounding zone for the Siple Coast is also thought to be relatively stable in comparison to other areas that have experienced rapid ice sheet thinning and grounding line retreat (Scheuchl et al., 2012). It is, thus, a suitable region for comparing data that were obtained at different times (e.g., from DInSAR and ICESat), and we do not need to account for changes in elevation due to nontidal processes.

We calculated T_d separately for POCA and swath data (Figure S1 in the supporting information), to account for any potential bias (Gray et al., 2017). We use the average value of T_d, if POCA and swath data produced a valid result for the same grid cell. In the fast-flowing areas of the Mercer, Whillans, and MacAyeal Ice Streams we obtained near complete coverage. Swath data were used in areas of high slope, but we still lost some coverage near the Transantarctic Mountains and Crary Ice Rise (Figure 2a). The map of T_d (Figure 2) and the cross sections of T_d across the Kamb and Mercer Ice Streams (Figure 2b) shows a clear change in dimensionless tidal amplitude between grounded and floating ice. Grounded ice has an average value of $T_d = 0.0 \pm 0.2$. In order to compare to other methods (e.g., DInSAR and ICESat), we considered the ice to be influenced by the vertical motion of the tides (i.e., point F) if it was 1 standard deviation above the grounded value or $T_d > 0.2$. We found this to be the most robust method to map F. Other methods such as fitting an appropriate function to the cross-slope shape, could potentially map F for $T_d = 0$, however, were unreliable.

Given the tidal range of the Ross Ice Shelf, defining point F as $T_d = 0.2$, corresponded to a minimum detectable vertical motion due to the tides of between ~20 and 40 cm. The higher precision of ICESat and DInSAR measurements (Brenner et al., 2007; Rignot, 1998; Schutz et al., 2005) allowed these methods to resolve smaller amplitude tidal variations. Therefore, when we compared the mapped grounding line to previous DInSAR observations (ESA Antarctic Ice Sheet Climate Change Initiative, 2017; Rignot et al., 2016) (Figure 3), we underestimated the landward distance to the grounding line by an average of 0.6 km. The bias was particularly apparent in the fast-flowing regions of the Mercer and Whillans Ice Streams where the transition from grounded to freely floating ice takes a greater distance and hence the gradient of T_d is lower (Figure 2b). Here we underestimated the landward distance by an average of 1.2 km compared to DInSAR measurements. In the slow flowing regions such as the Kamb Ice Stream and the Siple Dome the transition is much shorter and there was a bias of 0.4 km. This bias will be reduced if we could map the grounding line below its threshold value of $T_d = 0.2$. Nevertheless, the grounding line was of similar shape to the previous estimates (Figure 3), and this was reflected by the standard deviation between the CryoSat-2 grounding line and the DInSAR and ICESat (Brunt, Fricker, Padman, O'Neel, 2010) grounding lines of 1.1 km and 1.0 km, respectively. In comparison, the standard deviation between the ICEsat and DInSAR grounding line was 0.9 km.

The CryoSat-2-derived grounding line provides additional coverage on the Siple Coast. The new results indicate that the grounding line of the Echelmeyer Ice Stream is approximately 25 km inland from the previous estimates from ICESat (Figure 3a). There is, however, only one ICESat point which we could compare to, and we lose some coverage due to high slopes and wider track spacing of the satellite. If this difference was solely because the grounding line had retreated between the different epochs of the satellites (the ICESat and CryoSat-2 grounding line estimates used data from 2003 to 2008 and from 2010 to 2013, respectively), this would have resulted in an anomalously high retreat rate compared to rates observed elsewhere in Antarctica of up to 2 km/yr (Christie et al., 2016; Rignot et al., 2014; Scheuchl et al., 2016). It seems more likely that the ICESat pick is in error here, as there is a fairly extensive area of tidal motion inland of this point (Figure 3a). This error could have occurred partly because low surface slopes may lead to short term, tidally induced variability in the grounding line location (Milillo et al., 2017). ICESat could have sampled the grounding zone when the grounded ice extended further seaward. The grounding zone is also up to 5 km wide indicating that there

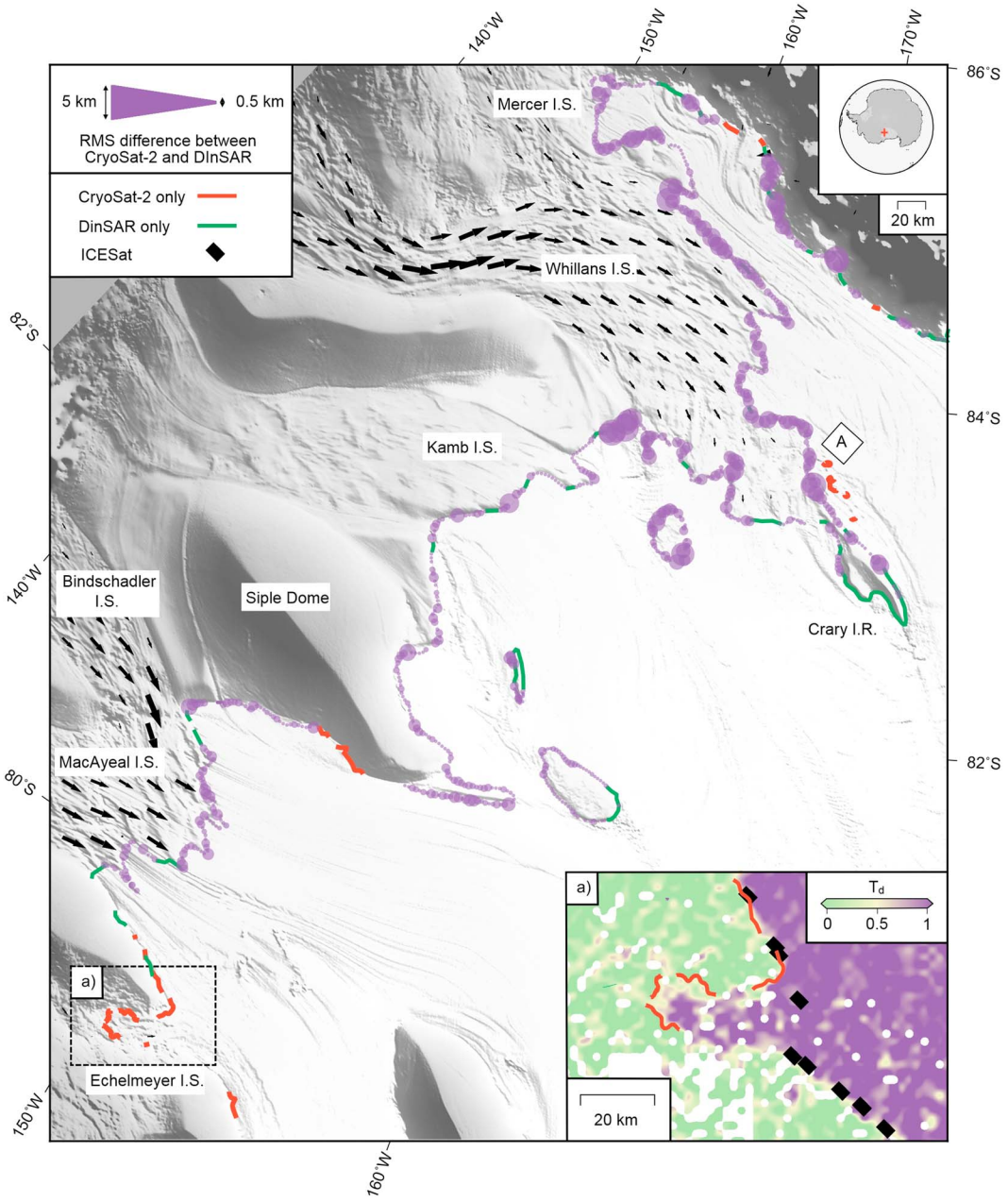

Figure 3. The root mean square (RMS) difference between the CryoSat-2 and DInSAR (ESA Antarctic Ice Sheet Climate Change Initiative, 2017; Rignot et al., 2016) mapped grounding lines for the Siple Coast region of the Ross Ice Shelf. Each purple circle represents the RMS distance between the two grounding line locations in 5 km bins along the grounding line. Red lines and green lines are where there is only CryoSat-2 or DInSAR data, respectively. Box A highlights an extra area of grounded ice, south of Crary Ice Rise. Insert a) shows the dimensionless tidal amplitude T_d for the Echelmeyer Ice Stream and the previous ICESat estimates (Brunt, Fricker, Padman, & O'Neel, 2010) (black diamonds). The grounding lines are overlain on a digital elevation model (DEM) created from same CryoSat-2 data used in this study. Areas of fast-flowing grounded ice are shown with black arrows (Rignot et al., 2011b, 2017). The place labels show ice streams (I.S.) and ice rises (I.R.)

is little variation in ice thickness (see section 4), which gives support to large tidally induced variability of the grounding line location in this area. In addition, at about 83.5°S, just south of Crary Ice Rise, there is a clear "tongue" (approximately 20 km long by 5 km wide) of grounded ice (labeled "A" in Figures 2 and 3). The wide track spacing of ICESat would make it difficult to resolve a feature of this size. However, it is also not identified by DInSAR data, which could indicate an evolution of grounded ice in this area.

4. Discussion

The potential for radar altimetry to identify the break-in-slope (point I) in the vicinity of the grounding zone was demonstrated more than 20 years ago (Bamber & Bentley, 1994). The aim of this study, however, was to assess the ability of CryoSat-2 to identify the grounding line using tidal flexure (point F) rather than break-in-slope. Point F lies close to the "true" grounding line (point G) and is less influenced by other factors such as ice rheology, thickness and motion (Bamber & Bently, 1994; Depoorter et al., 2013; Fricker & Padman, 2006; Rignot et al., 2011a). In principle, one of these factors could alter the location point of I without materially affecting the location of point G. Thus, for grounding line monitoring, it is more useful to identify changes in the position of point F than point I, and this is what has been done, to date, in almost all observationally based studies (e.g., Christie et al., 2016; Rignot et al., 2014; Scheuchl et al., 2016).

In a similar way to ICESat repeat track analysis (Fricker & Padman, 2006), the new method also allowed us to investigate the grounding zone beyond determining point F. As the dimensionless tidal amplitude measures the magnitude of the tidal contribution to elevation data, we can also detect point H by considering the ice to be in hydrostatic equilibrium if it is above a threshold value (e.g.,1 standard deviation below the average for freely floating ice or $T_d > 0.8$). This enabled us to measure the width of the grounding zone between points F and H (Fricker & Padman, 2006) providing information about its structure. For example, in Figure 2b, we show two cross sections of T_d, perpendicular to the slow flowing Kamb Ice Stream and the fast-flowing Mercer Ice Stream. The grounding zone is narrower across the Kamb Stream (1.5 km) as ice thickness increases more rapidly inland and bedrocks slope is higher compared to the fast-flowing Mercer Ice Stream where the grounding zone is 2.8 km wide.

To map F for the whole of the Antarctic grounding zones, using DInSAR is challenging, in part, due to the volume of SAR acquisitions needed and the processing requirements. Thus, a computationally and data efficient approach is highly desirable. CryoSat-2 has the potential to achieve this goal. The method presented here is computationally efficient, and while it is less sensitive to small amplitude tidal variations compared to ICESat and DInSAR methods, the accuracy of the grounding line location was similar between the different methods. The new method performed well on the Siple Coast region of the Ross Ice Shelf; however, several factors need to be considered in order to assess if this method can be extended to the rest of the Antarctic grounding zone.

The Siple Coast is at relatively high latitudes, with a track spacing of CryoSat-2 ranging from ~0.5 to ~1.5 km (Figure S1), and given the spatial sampling, using a 2 km cell size was sufficient to map the majority of the grounding zone. Grounding zones further north (e.g., along the Antarctic Peninsula, where the average track spacing can be as large as 4 km (Figure S1)), will have reduced data density. Coverage may also be lost in areas of high/rapidly varying surface slope, for example, near the Transantarctic mountains. In areas of low-latitude and high surface slope, swath data will be particularly important to improve the spatial coverage. However, the lower precision of swath data could limit the ability to resolve small tidal amplitudes, although this was not evident for our test region. Using a larger cell size will allow us to map more of the grounding zone in these areas, but with reduced accuracy.

It is also important to consider the tidal amplitude around Antarctica. We defined a minimum model tidal range of freely floating ice of 50 cm, and we were able to detect changes in vertical elevation due to the tides as low as ~20 cm in the grounding zone. This allowed us to resolve point F across the tidal range experienced across Ross Ice Shelf (~100 to 200 cm). The tidal range close to the grounding zone varies across Antarctica from ~80 cm near the Getz Ice Shelf to more than 400 cm for the Filchner Ronne Ice Shelf (Figure S1). This should allow us to resolve T_d for the majority of Antarctica. However, some areas may be below the sensitivity of the approach if CryoSat-2 does not sample the full tidal range, and the use of a longer time series could help resolve smaller tidal amplitudes.

The most problematic areas for our approach will be those farthest north with steeply sloping terrain and a small tidal range. Despite these limitations, we have been able to improve the coverage of the grounding zone in areas where there were no DInSAR data (Figure 2) and resolved small-scale features that were missed by ICESat. This included a region at the northern limit of our study area, near Echelmeyer Ice Stream, where we identified a likely error in the ICESat pick and an absence of DInSAR coverage. We achieved the best coverage in areas of fast flow, where the surface slope is relatively low. These areas are likely to have the most dynamic grounding line. In these regions the inland ice is close to flotation and the grounding line is therefore sensitive

to changes in ice thickness. While we lost some coverage in areas of high slope and slow flow, here the grounding line is relatively stable as ice thickness increases rapidly inland (e.g., Christie et al., 2016).

In this proof of concept study, we have only used 3 years of CryoSat-2 data and have not allowed for temporal grounding line migration or ice sheet thinning. Since CryoSat-2 has provided an almost continuous data set since July 2010, we can use the complete time series in order to provide quasi-annual sampling of the grounding zone and monitor changes in its location. Using a longer time series will require the use of snapshots of CryoSat-2 data at different epochs and the addition of time varying parameter (e.g., adding a linear surface elevation rate to equation (1)) to account for any nontidal changes. The epoch length we sample the grounding zone will depend on the tidal range and data coverage, and investigating how to monitor changes is an area for future development.

5. Conclusions

We presented a new method to map the grounding line using CryoSat-2 surface elevation measurements by determining the limit of tidal flexure of the floating ice as recorded in the altimeter data. This method adapts the pseudo crossover method of Wouters et al. (2015) and calculates a dimensionless tidal amplitude using an existing tide model. In this study we focus on mapping point F in order to compare it to previous methods. We are able to map the majority of the grounding zone of the Siple Coast region of the Ross Ice Shelf using this new method and obtain near complete coverage of low slope, fast-flowing areas, where grounding line migration is most likely to occur. The CryoSat-2 grounding line is in good agreement with previous methods, with a standard deviation of 1.1 km and 1.0 km compared to the DInSAR and ICESat grounding lines, respectively. However, the minimum tidal amplitude we can observe (~20 cm) is larger than the other methods discussed, leading to a bias ranging from 0.4 km to 1.2 km, as there is an underestimation of the landward distance to the grounding zone. This is particularly apparent in fast-flowing regions where the grounding zone is wider.

The additional coverage obtained using this method allows us to resolve new features, for example, the grounding line near the Echelmeyer Ice Stream is approximately 25 km inland from the previous grounding line estimate of ICESat. This method also provides additional information as it captures the tidal contribution to elevation data over the whole of the grounding zone. We can use this, for example, to measure the width of the grounding zone and provide additional information about its physical structure. While this method works best in high latitudes where there is denser data coverage, it should be possible to extend it to the rest of Antarctica. This will provide improved spatial and temporal coverage of the grounding zone over the lifetime of the satellite.

Acknowledgments
This work was supported by the UK Natural Environment Research Council (NERC) grant NE/N011511/1. The CryoSat-2 data used in this study are available from the European Space Agency (ESA). The DInSAR grounding line data are available from the National Snow and Ice Data Centre and the Centre for Environmental Data Analysis. The ICESat grounding line data are available the National Snow and Ice Data Centre. We thank L. Gray for his advice in processing the CryoSat-2 swath data. The authors are also grateful to Laurie Padman and an anonymous reviewer for their comments, which greatly improved this manuscript.

References

Bamber, J. L., & Bentley, C. R. (1994). A comparison of satellite-altimetry and ice-thickness measurements of the Ross Ice Shelf, Antarctica. *Annals of Glaciology*, *20*, 357–364.

Bamber, J. L., Gomez-Dans, J. L., & Griggs, J. A. (2009). A new 1 km digital elevation model of the Antarctic derived from combined satellite radar and laser data—Part 1: Data and methods. *The Cryosphere*, *3*, 101–111.

Bindschadler, R., Choi, H., Wichlacz, A., Bingham, R. G., Bohlander, J., Brunt, K. M., … Young, N. (2011). Getting around Antarctica: New high-resolution mappings of the grounded and freely-floating boundaries of the Antarctic ice sheet created for the International Polar Year. *The Cryosphere*, *5*, 569–588.

Bohlander, J., & Scambos, T. A. (2007). *Antarctic coastlines and grounding line derived from MODIS Mosaic of Antarctica (MOA)*. Boulder, CO: National Snow and Ice Data Center.

Brenner, A. C., DiMarzio, J. P., & Zwally, H. J. (2007). Precision and accuracy of satellite radar and laser altimeter data over the continental ice sheets. *IEEE Transactions on Geoscience and Remote Sensing*, *45*, 321–331.

Brunt, K. M., Fricker, H. A., Padman, L., & O'Neel, S. (2010). *ICESat-derived grounding zone for Antarctic ice shelves*. Boulder, CO: National Snow and Ice Data Center.

Brunt, K. M., Fricker, H. A., Padman, L., Scambos, T. A., & O'Neel, S. (2010). Mapping the grounding zone of the Ross Ice Shelf, Antarctica, using ICESat laser altimetry. *Annals of Glaciology*, *51*, 71–79.

Christie, F. D. W., Bingham, R. G., Gourmelen, N., Tett, S. F., & Muto, A. (2016). Four-decade record of pervasive grounding line retreat along the Bellingshausen margin of West Antarctica. *Geophysical Research Letters*, *43*, 5741–5749.

Depoorter, M. A., Bamber, J. L., Griggs, J. A., Lenaerts, J. T. M., Ligtenberg, S. R. M., van den Broeke, M. R., & Moholdt, G. (2013). Calving fluxes and basal melt rates of Antarctic ice shelves. *Nature*, *502*, 89–92.

ESA Antarctic Ice Sheet Climate Change Initiative (2017). Grounding line locations for the Ross and Byrd Glaciers, Antarctica, 2011–2017, v1.0. Centre for Environmental Data Analysis.

Fricker, H. A., & Padman, L. (2006). Ice shelf grounding zone structure from ICESat laser altimetry. *Geophysical Research Letters*, *33*, L15502.

Gray, L., Burgess, D., Copland, L., Cullen, R., Galin, N., Hawley, R., & Helm, V. (2013). Interferometric swath processing of Cryosat data for glacial ice topography. *The Cryosphere*, *7*, 1857–1867.

Gray, L., Burgess, D., Copland, L., Dunse, T., Langley, K., & Moholdt, G. (2017). A revised calibration of the interferometric mode of the CryoSat-2 radar altimeter improves ice height and height change measurements in western Greenland. *The Cryosphere*, *11*, 1041–1058.

Gray, L., Short, N., Bindschadler, R., Joughin, I., Padman, L., Vornberger, P., & Khananian, A. (2002). RADARSAT interferometry for Antarctic grounding-zone mapping. *Annals of Glaciology*, *34*, 269–276.

Helm, V., Humbert, A., & Miller, H. (2014). Elevation and elevation change of Greenland and Antarctica derived from CryoSat-2. *The Cryosphere*, *8*, 1539–1559.

Hogg, A. E., Shepherd, A., Gilbert, L., Muir, A., & Drinkwater, M. R. (2017). Mapping ice sheet grounding lines with CryoSat-2. *Advances in Space Research*. https://doi.org/10.1016/j.asr.2017.03.008

McMillan, M., Shepherd, A., Sundal, A., Briggs, K., Muir, A., Ridout, A., & Wingham, D. (2014). Increased ice losses from Antarctica detected by CryoSat-2. *Geophysical Research Letters*, *41*, 3899–3905.

Milillo, P., Rignot, E., Mouginot, J., Scheuchl, B., Morlighem, M., Li, X., & Salzer, J. T. (2017). On the short-term grounding zone dynamics of Pine Island Glacier, West Antarctica, observed with COSMO-SkyMed interferometric data. *Geophysical Research Letters*, *44*, 10,436–10,444. https://doi.org/10.1002/2017GL074320

Mouginot, B., Scheuchl, J., & Rignot, E. M. (2017). *MEaSUREs Antarctic boundaries for IPY 2007–2009 from satellite radar, version 2*. Boulder, CO: NASA DAAC at the National Snow and Ice Data Center.

Padman, L., Erofeeva, S. Y., & Fricker, H. A. (2008). Improving Antarctic tide models by assimilation of ICESat laser altimetry over ice shelves. *Geophysical Research Letters*, *35*, L22504.

Padman, L., Fricker, H. A., Coleman, R., Howard, S., & Erofeeva, L. (2002). A new tide model for the Antarctic ice shelves and seas. *Annals of Glaciology*, *34*, 247–254.

Rignot, E. (1998). Hinge-line migration of Petermann Gletscher, north Greenland, detected using satellite-radar interferometry. *Journal of Glaciology*, *44*, 469–476.

Rignot, E., Jacobs, S., Mouginot, J., & Scheuchl, B. (2013). Ice-shelf melting around Antarctica. *Science*, *341*, 266–270.

Rignot, E., Mouginot, J., Morlighem, M., Seroussi, H., & Scheuchl, B. (2014). Widespread, rapid grounding line retreat of Pine Island, Thwaites, Smith, and Kohler glaciers, West Antarctica, from 1992 to 2011. *Geophysical Research Letters*, *41*, 3502–3509.

Rignot, E., Mouginot, J., & Scheuchl, B. (2011a). Antarctic grounding line mapping from differential satellite radar interferometry. *Geophysical Research Letters*, *38*, L10504.

Rignot, E., Mouginot, J., & Scheuchl, B. (2011b). Ice flow of the Antarctic ice sheet. *Science*, *333*, 1427–1430.

Rignot, E., Mouginot, J., & Scheuchl, B. (2016). *MEaSUREs Antarctic grounding line from differential satellite radar interferometry, version 2*. Boulder, CO: NASA National Snow and Ice Data Center Distributed Active Archive Center. Accessed on 4 September 2016.

Rignot, E., Mouginot, J., & Scheuchl, B. (2017). *MEaSUREs InSAR-based Antarctica ice velocity map, version 2*. Boulder, CO: NASA DAAC at the National Snow and Ice Data Center.

Scheuchl, B., Mouginot, J., & Rignot, E. (2012). Ice velocity changes in the Ross and Ronne sectors observed using satellite radar data from 1997 and 2009. *The Cryosphere*, *6*, 1019–1030.

Scheuchl, B., Mouginot, J., Rignot, E., Morlighem, M., & Khazendar, A. (2016). Grounding line retreat of Pope, Smith, and Kohler Glaciers, West Antarctica, measured with Sentinel-1a radar interferometry data. *Geophysical Research Letters*, *43*, 8572–8579.

Schutz, B. E., Zwally, H. J., Shuman, C. A., Hancock, D., & DiMarzio, J. P. (2005). Overview of the ICESat mission. *Geophysical Research Letters*, *32*, L21S0.

Shepherd, A., Wingham, D. J., & Mansley, J. A. D. (2002). Inland thinning of the Amundsen Sea sector, West Antarctica. *Geophysical Research Letters*, *29*, 1364.

Wang, F., Bamber, J. L., & Cheng, X. (2015). Accuracy and performance of CryoSat-2 SARIn mode data over Antarctica. *IEEE Geoscience and Remote Sensing Letters*, *12*, 1516–1520.

Wouters, B., Martin-Español, A., Helm, V., Flament, T., van Wessem, J. M., Ligtenberg, S. R. M., … Bamber, J. L. (2015). Dynamic thinning of glaciers on the Southern Antarctic Peninsula. *Science*, *348*, 899–903.